JACS
JOURNAL OF THE AMERICAN CHEMICAL SOCIETY
pubs.acs.org/JACS
Article

Tailoring Interfaces for Enhanced Methanol Production from Photoelectrochemical CO_2 Reduction

Bo Shang,[○] Fengyi Zhao,[○] Sa Suo, Yuanzuo Gao, Colton Sheehan, Sungho Jeon, Jing Li, Conor L. Rooney, Oliver Leitner, Langqiu Xiao, Hanqing Fan, Menachem Elimelech, Leizhi Wang, Gerald J. Meyer, Eric A. Stach, Thomas E. Mallouk, Tianquan Lian,* and Hailiang Wang*

Cite This: *J. Am. Chem. Soc.* 2024, 146, 2267−2274

Read Online

ACCESS | Metrics & More | Article Recommendations | Supporting Information

ABSTRACT: Efficient and stable photoelectrochemical reduction of CO_2 into highly reduced liquid fuels remains a formidable challenge, which requires an innovative semiconductor/catalyst interface to tackle. In this study, we introduce a strategy involving the fabrication of a silicon micropillar array structure coated with a superhydrophobic fluorinated carbon layer for the photoelectrochemical conversion of CO_2 into methanol. The pillars increase the electrode surface area, improve catalyst loading and adhesion without compromising light absorption, and help confine gaseous intermediates near the catalyst surface. The superhydrophobic coating passivates parasitic side reactions and further enhances local accumulation of reaction intermediates. Upon one-electron reduction of the molecular catalyst, the semiconductor−catalyst interface changes from adaptive to buried junctions, providing a sufficient thermodynamic driving force for CO_2 reduction. These structures together create a unique microenvironment for effective reduction of CO_2 to methanol, leading to a remarkable Faradaic efficiency reaching 20% together with a partial current density of 3.4 mA cm^{-2}, surpassing the previous record based on planar silicon photoelectrodes by a notable factor of 17. This work demonstrates a new pathway for enhancing photoelectrocatalytic CO_2 reduction through meticulous interface and microenvironment tailoring and sets a benchmark for both Faradaic efficiency and current density in solar liquid fuel production.

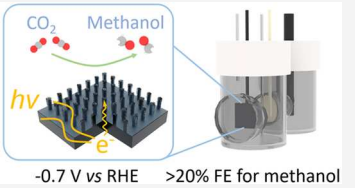

INTRODUCTION

The reduction of carbon dioxide (CO_2) into liquid fuels with renewable energy represents a promising solution to both combat greenhouse gas emissions and store renewable energy.[1,2] Photoelectrocatalysis has emerged as an efficient method to harness solar energy and facilitate CO_2 electroreduction at low applied voltages.[3−6] In a typical photoelectrocatalytic (PEC) CO_2 reduction process, a semiconductor absorbs light to generate excited electrons, which are transferred by a catalyst to CO_2. Among the various semiconductor materials investigated, Si-based photocathodes have garnered attention due to their cost-effectiveness, solar light harvesting, and well-understood properties.[7,8] Molecular catalysts, particularly transition metal complexes, are viable options for catalyzing the CO_2 reduction reaction, offering high selectivity and tunable catalytic properties.[9−11] Previous studies have achieved successful CO_2 reduction to CO and formate using Si-based photocathodes combined with molecular catalysts.[7,12,13] However, achieving efficient and stable PEC CO_2 reduction to more highly reduced liquid fuels remains an important challenge.[14−16]

In our prior work, we explored a TiO_2-coated planar p-type Si substrate integrated with a cobalt phthalocyanine (CoPc)/graphene oxide (GO) hybrid catalyst via a molecular linker.[15] Although this photocathode demonstrated the ability to achieve six-electron reduction of CO_2 to methanol with a Faradaic efficiency (FE) of 8%, the current density and stability were limited, likely due to the relatively low catalytic performance of GO/CoPc and weak interactions with the Si substrate. To improve the PEC performance, successful integration of a better optimized catalyst on Si is desired and requires addressing several challenges in fundamental energy research that include: (1) stabilization of the catalyst on the Si surface through covalent linking or self-assembly; (2) identification of the ideal catalyst surface loading for optimal catalysis and minimal light absorption; (3) passivation of the native Si surface to inhibit hydrogen evolution reaction (HER); (4) tailoring of the interfacial energetics to provide the thermodynamic driving force necessary for rapid interfacial electron transfer; (5) creation of a hydrophobic interfacial environment to tailor reaction selectivity toward methanol. These five challenges can be overcome through critical control of the interface between the Si light absorber and the molecular catalyst.[17]

In this paper, we report the achievement of PEC CO_2 reduction to methanol with over 20% FE, a remarkable partial photocurrent density of 3.4 mA cm^{-2}, and a high turnover

Received: December 3, 2023
Revised: December 14, 2023
Accepted: December 18, 2023
Published: January 11, 2024

Downloaded via UNIV OF PENNSYLVANIA on March 19, 2024 at 16:03:19 (UTC).
See https://pubs.acs.org/sharingguidelines for options on how to legitimately share published articles.

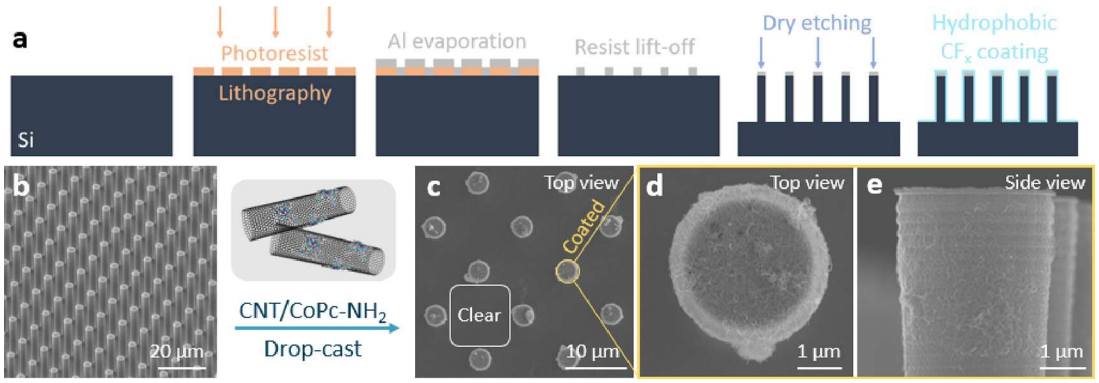

Figure 1. (a) SMA fabrication and CF_x coating. (b) SEM image of SMA-CF_x. (c) SEM image of SMA-CF_x coated with the CNT/CoPc-NH_2 catalyst. (d, e) Top-view and side-view SEM images of a single SMA-CF_x pillar coated with CNT/CoPc-NH_2.

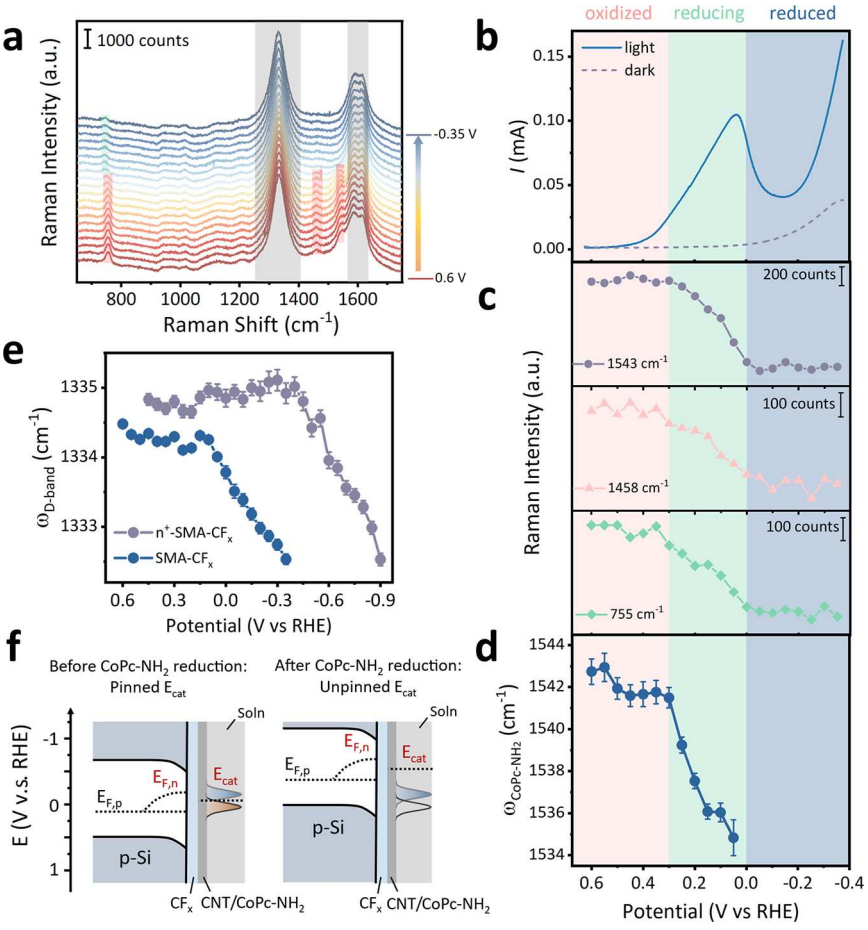

Figure 2. (a) In situ Raman spectra of CNT/CoPc-NH_2 on SMA-CF_x from 0.625 to −0.375 V under 632.8 nm illumination. (b) Linear sweep voltammograms of SMA-CF_x-CNT/CoPc-NH_2 measured in the dark and during in situ Raman measurement. (c) One-electron reduction of CoPc-NH_2 tracked by changes in resonance Raman intensity. Potential-dependent Raman vibrational frequencies of the (d) CoPc-NH_2 1543 cm^{-1} peak and (e) CNT D band. (f) Proposed band diagram at SMA-CF_x-CNT/CoPc-NH_2-solution interfaces. The electrode was tested after preconditioning the electrode at −0.5 V for 10 min under 150 mW cm^{-2} Xe lamp irradiation. The red, blue, and green shaded potential regions in panels (b), (c), and (d) indicate the potential ranges of oxidized, reduced, and mixed CoPc-NH_2 species, respectively, as determined from the Raman data shown in panel (c).

frequency (TOF) of 1.5 s^{-1}. This stands as the highest performance reported to date for any molecular catalyst-based photoelectrode. The enhancement in performance was realized by designing the semiconductor/catalyst interface and tailoring the electrode microenvironment, which plays a critical role in optimizing the cascade of CO_2 reduction to methanol. We fabricated the p-type Si substrate surface into an array of micropillars, which enabled the effective integration of a carbon nanotube/amine-substituted CoPc (CNT/CoPc-NH_2) catalyst without sacrificing light absorption as well as improved retention of the key CO intermediate. This Si micropillar array (SMA) photoelectrode yielded a 1.6-fold increase in total current density and a 1.5-fold increase in $FE_{methanol}$ compared to a previously reported planar Si electrode with the GO/CoPc

https://doi.org/10.1021/jacs.3c13540
J. Am. Chem. Soc. 2024, 146, 2267−2274

catalyst.[15] We further introduced a superhydrophobic carbon fluoride (CF_x) coating on the SMA substrate to enhance the conversion of the gaseous reactant and intermediate. This microenvironment led to another 2-fold increase in $FE_{methanol}$ and, more remarkably, an additional 7-fold increase in the methanol partial current density. In situ Raman spectroscopy revealed ~300 mV of photovoltage from SMA and a transition from adaptive to buried semiconductor/catalyst junctions with a negative applied potential, further deepening our mechanistic understanding of the SMA-CNT/CoPc-NH_2 interface.

RESULTS AND DISCUSSION

The SMA structure with a pillar diameter of 3 μm, a pillar height of 18 μm, and a pitch of 10 μm was fabricated through photolithography and dry etching (Figures 1a and S1). Following the etching step, a thin CF_x layer was coated on SMA using octafluorocyclobutane (C_4F_8) plasma. Subsequently, the CNT/CoPc-NH_2 catalyst was drop-casted onto the SMA-CF_x substrate (Figures 1b,c and S2). Due to the hydrophobic nature of the SMA-CF_x surface, the CNT/CoPc-NH_2 catalyst exhibits a preference for adhering to the top and sides of the Si pillars rather than the flat basal plane of the substrate (Figure 1c–e), likely as a result of surface tension of the catalyst ink. This distinct assembly pattern leaves approximately 90% of the geometrical area free of the strongly absorbing black CNTs for more optimal solar light harvesting by the Si substrate.

To directly probe how the quasi-Fermi level of the CNT/CoPc-NH_2 catalyst changes with applied potential under illumination, the SMA-CF_x-CNT/CoPc-NH_2 photoelectrode was characterized by in situ Raman spectroscopy in CO_2-saturated 0.1 M aqueous $KHCO_3$ (pH 6.8) using a 632.8 nm He–Ne laser as both a Raman probe and an illumination source.[18] A representative set of potential dependent Raman spectra is shown in Figure 2a. Linear sweep voltammetry (LSV) at a scan rate of 1.7 mV/s from 0.625 to −0.375 V (Figure 2b) versus the reversible hydrogen electrode (RHE, all potentials in this work are referenced to RHE unless otherwise stated) was conducted in the dark and in the light, the latter being concurrent with Raman spectrum acquisition. Resonance Raman features of CoPc-NH_2 were observed at 755, 1458, and 1543 cm^{-1} (red shade in Figure 2a).[19−21] The peaks at 1334, 1585, and 1617 cm^{-1} correspond to CNT's D, G^-, and G^+ bands (gray shade in Figure 2a), respectively.[22,23] Our initial focus was to monitor the resonant Raman peaks of CoPc-NH_2 as a function of applied potential, whose intensity is known to decrease upon one-electron reduction of the CoPc-NH_2 molecule.[19,20] As the applied potential is polarized toward the negative direction, the CoPc-NH_2 resonances start to decrease in magnitude at 0.3 V, and the decrease levels off after the potential reaches 0 V (Figure 2c), suggesting that the CoPc-NH_2 molecules undergo one-electron reduction in this potential range. A photoelectrochemical reduction wave was consistently observed in this potential range, reaching a peak current at 0.05 V (Figure 2b). Starting at 0 V, a new Raman peak was observed at 746 cm^{-1} (green shade in Figure 2a and Figure S3), which is attributed to the reduced CoPc-NH_2. In a control experiment, the electrochemical reduction of CNT/CoPc-NH_2 deposited on a degenerately doped n-type SMA-CF_x (n^+-SMA-CF_x) substrate was quantified (Figure S4). The resonant Raman peaks of CoPc-NH_2 did not reach their lowest intensity until about −0.3 V, which, in comparison with the corresponding SMA-CF_x-CNT/CoPc-NH_2 results (Figure 2c), suggests a 300 mV photovoltage, that is, quasi-Fermi-level splitting for the p-type SMA electrode.

Further details about the CNT/CoPc-NH_2 catalyst were obtained through fitting of the CNT D, G^+, and G^- bands as well as the 1458 and 1543 cm^{-1} peaks of CoPc-NH_2 (Figure S5). The frequency of the CoPc-NH_2 1543 cm^{-1} peak ($\omega_{CoPc\text{-}NH2}$) exhibits intriguing potential-dependent behavior. At potentials above 0.3 V, the frequency was unchanged and decreased continuously with increasing reducing potential in the 0.3–0 V range (Figure 2d). The measured $\omega_{CoPc\text{-}NH2}$ shift is attributed to the potential-dependent electric field at the CNT/CoPc-NH_2-electrolyte interface that affects the CoPc-NH_2 frequency through a Stark-like effect or the electro-inductive effect on CoPc-NH_2 molecules induced by a change in the CNT Fermi level.[24−26] Of the three observed vibrational modes of CoPc-NH_2, the 1543 cm^{-1} peak, assigned to the C_α-N_β-C_α bridging bond displacement, was the only one that displayed a significant potential-dependent frequency shift. This may be resulted from the macrocycle plane's rotation along the C_α-N_β-C_α bridge that generates a dipole moment perpendicular to the CNT surface.[26] The other two modes, however, mainly generate dipole moments within the molecular plane.[21,27]

The frequency of the CNT D band ($\omega_{D\text{-}band}$) has been shown to be sensitive to the Fermi level of the material and can be used as a reporter of chemical and electrochemical doping.[23,28,29] Interestingly, $\omega_{D\text{-}band}$ shows potential-dependent behavior similar to the 1543 cm^{-1} peak of CoPc-NH_2. As the applied potential is swept cathodically from 0.625 to −0.375 V, $\omega_{D\text{-}band}$ remains constant until ~0.1 V and then decreases (Figure 2e). We attribute this to a shift of the CNT quasi-Fermi level at ~0.1 V for CNT/CoPc-NH_2 on SMA-CF_x under photoelectrochemical conditions. For CNT/CoPc-NH_2 integrated with n^+-SMA-CF_x, a similar potential-dependent $\omega_{D\text{-}band}$ trend was observed, but the onset of $\omega_{D\text{-}band}$ frequency shift occurs at −0.3 V (gray trace in Figure 2e). It is worth noting that although the shift of $\omega_{D\text{-}band}$ reports on the change of CNT Fermi level, it is difficult to establish a universal calibration curve that relates the $\omega_{D\text{-}band}$ value to the Fermi level (Figure S6 and Table S1) because the D band frequency is not only sensitive to the electric field but also to solution microenvironment factors such as chemisorption of electrolyte ions and local pH changes.[28,30,31]

Based on the above analysis, we propose the following properties for the SMA-CF_x-CNT/CoPc-NH_2-solution junction. As summarized in Figure 2f, the potentiostat controls the hole Fermi level of Si ($E_{F,p}$), the quasi-Fermi level of electrons ($E_{F,n}$) shifts to higher energy upon photogeneration and separation of electrons, and the Fermi level of CNT and the attached CoPc-NH_2 molecules equilibrate with each other, denoted as E_{cat}. From the Si flat-band potential to 0.1 V (left panel of Figure 2f), E_{cat} is pinned by the one-electron reduction potential of CoPc-NH_2, which means that the applied potential mainly drops on the semiconductor side, providing the electric field needed to separate the photogenerated charge carriers and generating a photovoltage of ~300 mV to reduce the CoPc-NH_2 molecules. When the applied potential becomes more negative than 0.1 V (right panel of Figure 2f), E_{cat} is unpinned as the molecules are reduced. In this potential region, the semiconductor band bending and the height of the semiconductor–catalyst barrier remain constant, irrespective of the applied potential. The applied potential change ($\Delta E_{F,p}$) directly shifts E_{cat} toward

https://doi.org/10.1021/jacs.3c13540
J. Am. Chem. Soc. 2024, 146, 2267−2274

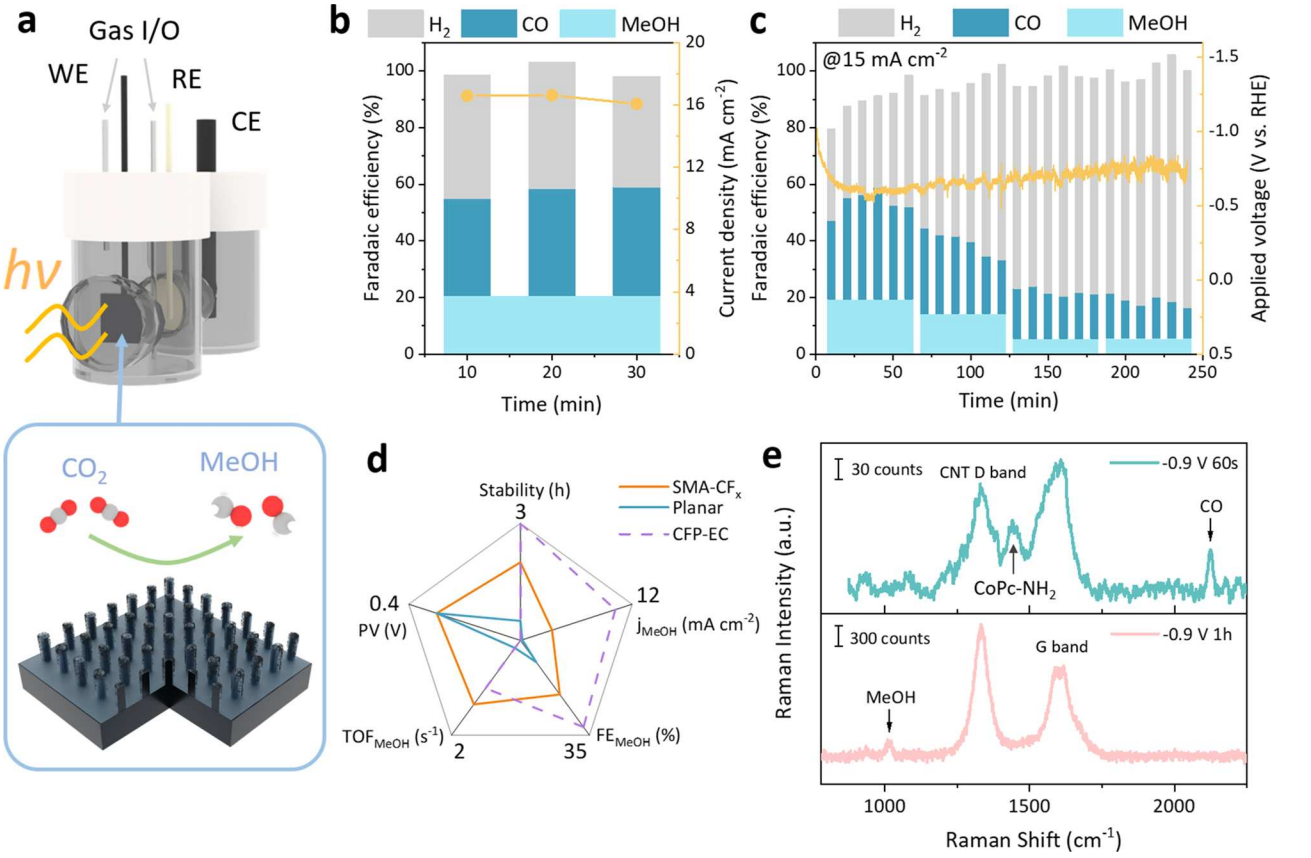

Figure 3. PEC CO_2 reduction performance of SMA-CF_x-CNT/CoPc-NH_2 in 0.1 M aqueous $KHCO_3$ under illumination. (a) PEC cell structure. (b) Total photocurrent and product distribution at −0.7 V. CO and H_2 were sampled every 10 min, whereas the methanol concentration was measured after the 30 min reaction to report its average FE. (c) Stability test at a constant photocurrent of 15 mA cm^{-2}, showing the applied potential needed to maintain the constant photocurrent (yellow line, right axis) and the FEs for H_2, CO, and methanol (vertical bars, left axis) as a function of time. (d) Performance comparison with GO/CoPc-functionalized planar Si (under illumination) and CNT/CoPc-NH_2 deposited on carbon fiber paper for electrocatalysis (CFP-EC, electrolysis without illumination). (e) In situ Raman measurements at 60 s (top) and 1 h (bottom) into photoelectrolysis at −0.9 V, showing generated CO and methanol.

more negative potential. The junction properties in terms of pinned and unpinned E_{cat} are also known as "adaptive" and "buried" junctions, respectively, according to the literature.[32−35] The formation of the buried junction results in an electrostatic potential drop across the solution double layer, which could render a suitable microenvironment for the reduction of CO_2 at more negative potentials. Our result suggests efficient electron tunneling from SMA to CNT/CoPc-NH_2 in this architecture.

The performance of the fabricated photoelectrode for PEC CO_2 reduction was evaluated in CO_2-saturated 0.1 M aqueous $KHCO_3$ by using an H-cell with a quartz window under the illumination of an Xe lamp (150 mW cm^{-2}, 400 nm cutoff), as depicted in Figure 3a. All constant potential photoelectrolysis experiments were conducted after preconditioning the electrode at −0.5 V under illumination for 10 min. The current increases and then stabilizes during the preconditioning (Figure S7), which is possibly due to the dissolution of the insulating native oxide layer on Si. In situ Raman spectroscopy measurement of unconditioned SMA-CF_x-CNT/CoPc-NH_2 shows reduction of CoPc-NH_2 and electron doping of CNTs similar to that on the preconditioned photoelectrode but at more cathodic potentials (Figure S8). By comparing the CoPc-NH_2 reduction and $\omega_{D\text{-band}}$ shifting potentials between these two conditions, we find that the preconditioning could reduce the interfacial potential loss by about 200 mV, likely by reducing the surface oxide or passivating the surface states on Si and thus decreasing the interfacial resistance. Under −0.7 V applied potential (after preconditioning), the SMA-CF_x-CNT/CoPc-NH_2 photocathode delivers a methanol FE of 21% and a CO FE of 37%, accompanied by a total photocurrent of 16.6 mA cm^{-2} (Figure 3b). A photovoltage of ∼350 mV is gained from the Si substrate, as inferred from the maximum-$FE_{methanol}$ potential difference with versus without illumination (Figure S9), which matches the in situ Raman results (Figures 2c and S4). The stability of SMA-CF_x-CNT/CoPc-NH_2 was evaluated under constant current mode with a photocurrent of 15 mA cm^{-2} (Figure 3c). In the first 20 min, the applied potential drops continuously, which is similar to the activation observed in the preconditioning step under the constant potential mode. After that, a stable FE of ∼20% for methanol is achieved and maintained for 2 h. Subsequently, $FE_{methanol}$ decreases to 6%, accompanied by an increase in the partial current density of H_2, which may be attributed to the exposure of the Si surface to the electrolyte.

Comparison of performance for CO_2 reduction to methanol, in terms of stability, partial current density, FE, TOF, and photovoltage, is made between different CoPc-based (photo)-electrodes (Figure 3d). The SMA-CF_x-CNT/CoPc-NH_2 photoelectrode has arguably the best overall performance. It exhibits a similar photovoltage of ∼350 mV but 3, 17, and 4 times higher FE, methanol production rate, and stable

https://doi.org/10.1021/jacs.3c13540
J. Am. Chem. Soc. 2024, 146, 2267−2274

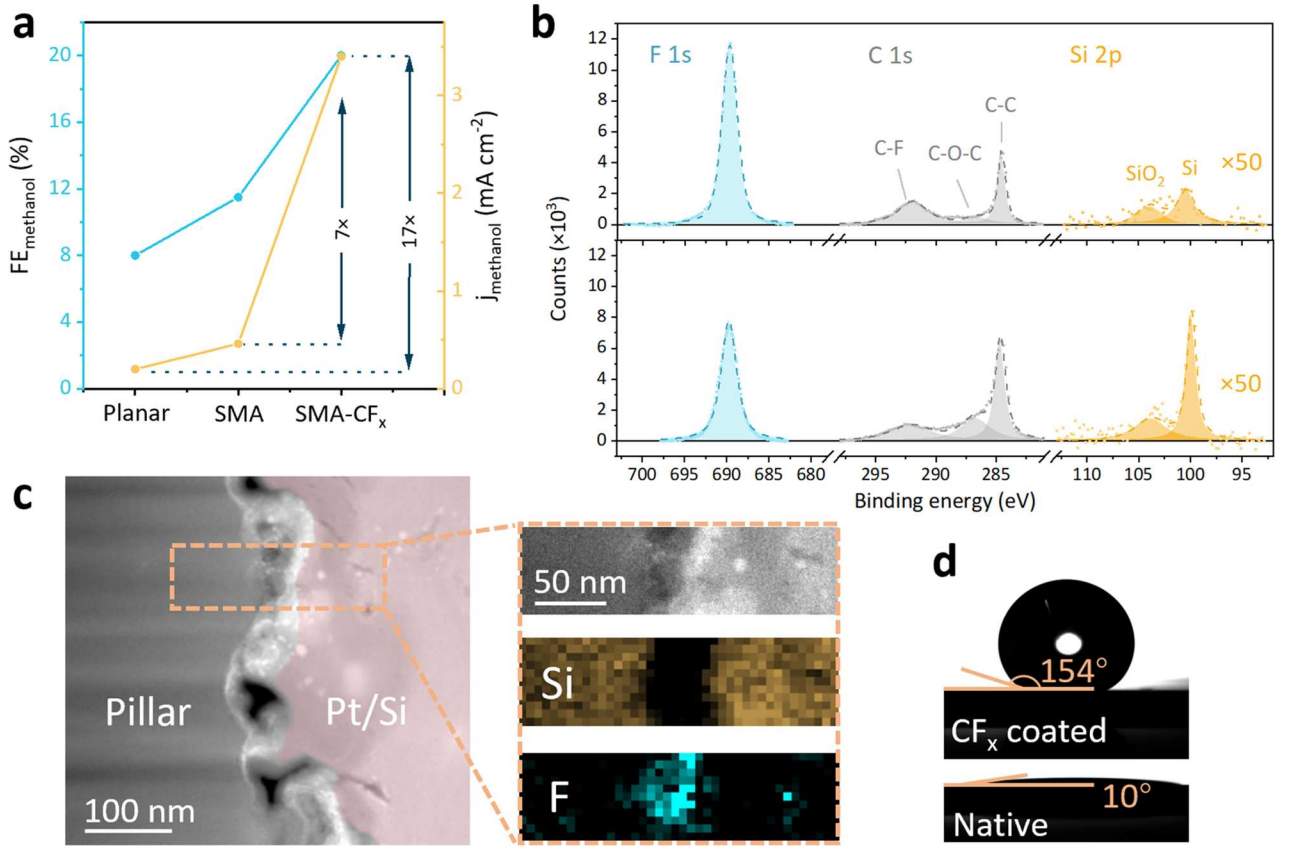

Figure 4. (a) Comparison of methanol selectivity and partial current density between SMA-CF$_x$-CNT/CoPc-NH$_2$ (noted as SMA-CF$_x$), SMA-CNT/CoPc-NH$_2$ (noted as SMA), and planar Si-TiO$_2$-GO/CoPc (noted as planar). (b) XPS spectra of SMA-CF$_x$-CNT/CoPc-NH$_2$ before (upper panel) and after (lower panel) 4 h of PEC CO$_2$ reduction. (c) Cross-section STEM image of a single Si pillar and STEM-EDS mapping of the boxed area. Pt/Si (false colored) was deposited onto the pillar sidewall to prepare the thin slice with FIB. (d) Contact angle measurements on the SMA-CF$_x$ and SMA.

operation time, respectively, than our prior generation of photoelectrodes based on planar Si and the GO/CoPc catalyst.[15] Compared with the state-of-the-art electrode of CNT/CoPc-NH$_2$ deposited on CFP (Figure S10), the SMA-CF$_x$-CNT/CoPc-NH$_2$ photoelectrode has the advantage of improved overpotential because of the photovoltage but is about 1.3 times lower in FE and 3 times lower in partial current density (Figure 3d).[9] The lower methanol selectivity and production rate may be attributed to a lower catalyst loading (0.1 mg cm^{-2} on SMA vs 0.4 mg cm^{-2} on CFP) and less effective CO$_2$ mass transport (the hydrophobic CFP substrate resembles a gas diffusion electrode). Both are limitations that need to be solved in future work to further improve the PEC performance. Interestingly, the TOF for methanol production on SMA-CF$_x$-CNT/CoPc-NH$_2$ reaches approximately 1.5 s^{-1}, largely comparable to that achieved in CNT/CoPc-NH$_2$-catalyzed electrolysis (1.0 s^{-1}) if the different catalyst loadings are taken into consideration. CO$_2$ reduction intermediates and products are also detected by Raman spectroscopy as shown in Figure 3e. After 60 s into photoelectrolysis under −0.9 V applied potential, a peak at 2120 cm^{-1} evolves (green, upper panel), confirming the formation of free CO bubbles on the surface.[36] A peak at 1015 cm^{-1} appears after 1 h of reaction and product accumulation (pink, lower panel). This peak is assigned to methanol's C−O stretching (Figure S11),[37] confirming the generation of methanol as a product. The 2120 cm^{-1} CO peak is not detected in this spectrum, likely because loosely bound CO bubbles detach from the electrode.

The improved methanol production performance of the SMA-CF$_x$-CNT/CoPc-NH$_2$ photoelectrode is a result of the micropillar array structure and the CF$_x$ coating. The SMA-CNT/CoPc-NH$_2$ photoelectrode (without CF$_x$) shows 1.5 times the FE and 2.3 times the partial current density of the planar Si-GO/CoPc electrode (Figure 4a), demonstrating the effect of the SMA surface. Considering that CO is the key reaction intermediate on the CO$_2$-to-methanol pathway that easily desorbs from the CoPc catalytic site,[38−40] we hypothesize that the micropillar array structure can help retain CO microbubbles between the pillars and thus enhance their further reduction to generate methanol. This hypothesis is supported by our simulation results showing that the micropillar array structure can retain over 1.5 times the local CO concentration compared to the planar surface under identical CO generation fluxes (Figure S12). This hypothesis is also consistent with our experimental observation that the height and pitch of the micropillar array influence methanol selectivity and photocurrent. Considerably lower FE$_{methanol}$ and slightly lower total current density are observed for SMA with a shorter pillar height of 7 μm (Figure S13a,b). This may be due to a reduced CO trapping capability and lower electrode surface area. A larger pillar height of 36 μm does not seem to affect methanol production much but significantly increase the HER rate likely because of a larger area of exposed Si surface

https://doi.org/10.1021/jacs.3c13540
J. Am. Chem. Soc. 2024, 146, 2267−2274

(Figure S13c,d).[8,15,41] For a similar reason, a smaller pitch of 8 μm also elevates H_2 evolution (Figure S13a,c).

The CF_x coating is also key to the enhanced PEC performance. X-ray photoelectron spectroscopy (XPS) successfully detected F and F-bonded C together with a little Si (Figure 4b, upper panel), confirming the presence of CF_x on the photoelectrode surface. To characterize the thickness and uniformity of the CF_x layer, we used a focused ion beam (FIB) to slice a thin layer (approximately 100 nm thick) off a pillar, as illustrated in Figures 4c and S14. Scanning transmission electron microscopy (STEM) and energy-dispersive X-ray spectroscopy (EDS) were performed on the slice. A continuous F-containing layer with an average thickness of ∼40 nm was observed (Figures 4c and S15), suggesting that a CF_x layer of the same thickness effectively covered the Si surface. With this coating, the SMA-CF_x substrate exhibits superhydrophobic properties with an ultrahigh contact angle of 154° with water, while the CF_x-free SMA (native oxide surface) shows a low contact angle of only 10° (Figures 4d and S16 and Video S1). Incorporation of CF_x into the SMA-CNT/CoPc-NH_2 structure increases the CO_2 reduction current by 4 times and the $FE_{methanol}$ by 1.8 times, leading to a 7-fold increase in the methanol production rate (Figures 4a and S13a). In a control experiment, an SMA-TiO_2−CNT/CoPc-NH_2 photoelectrode exhibits a lower photocurrent (∼7 mA cm^{-2}), a lower methanol FE (14%), and a much higher H_2 FE (71%) than SMA-CF_x-CNT/CoPc-NH_2 (Figure S17). This comparison reflects the roles of the hydrophobic CF_x layer. It can facilitate CO_2 mass transport, enhance CO retention, and suppress electrolyte penetration into the interspace of the micropillars, leading to improved CO_2 reduction to methanol and suppressed H_2 evolution.[42]

As the methanol production performance of the SMA-CF_x-CNT/CoPc-NH_2 photoelectrode starts to decay after 2 h of operation (Figure 3c), we further examined a used photoelectrode (after 4 h of PEC test at 15 mA cm^{-2}) to understand the deactivation. Compared to the fresh photoelectrode, the deactivated photoelectrode has considerably less F and more Si on the surface, as revealed by XPS (Figure 4b and Table S2), indicating that the CF_x coating layer has degraded after the long-term PEC test. This change in surface composition can explain the observed deactivation behavior. The degradation of the CF_x layer leads to a lowered surface hydrophobicity, which lessens the reduction of CO_2 to methanol. On the other hand, the newly exposed Si surface facilitates HER.[8,15,41] We note that suppressing the HER on Si photoelectrodes, especially during long-term operation, remains challenging. It is limited by the trade-off between catalyst coverage/loading and light absorption as well as the durability of the surface passivation layer under reaction conditions. The highly reducing condition required for methanol production is a big threat to traditional metal oxide passivation layers like TiO_2,[15] and even CF_x is not adequate. Future work is needed to solve this problem.[43]

CONCLUSIONS

In conclusion, our study successfully showcases the effectiveness of microenvironment and interface tailoring on Si-based CO_2 reduction photocathodes, leading to a remarkable FE of over 20% for methanol production with a record-high partial current density. The incorporation of the micropillar array structure and the superhydrophobic CF_x coating plays a crucial role in enhancing retention of the CO intermediate, consequently improving the selectivity toward the deeply reduced methanol product. The unique Si-molecular catalyst buried junction efficiently converts absorbed photon energy into the chemical driving force for CO_2 reduction. This work pioneers a route for microenvironment tailoring on semiconductor surfaces and establishes a new benchmark for PEC CO_2 reduction to liquid fuel using molecular catalysts. The insights gained from this research hold promise for driving further developments in the quest for sustainable and efficient utilization of carbon emissions.

ASSOCIATED CONTENT

Supporting Information

The Supporting Information is available free of charge at https://pubs.acs.org/doi/10.1021/jacs.3c13540.

Superhydrophobicity of SMA (MP4)

Materials, catalyst ink preparation, photoelectrode fabrication, photoelectrochemical measurements, characterization methods, numerical modeling method, and supplementary figures and tables (PDF)

AUTHOR INFORMATION

Corresponding Authors

Tianquan Lian − *Department of Chemistry, Emory University, Atlanta, Georgia 30322, United States;* orcid.org/0000-0002-8351-3690; Email: tlian@emory.edu

Hailiang Wang − *Department of Chemistry, Yale University, New Haven, Connecticut 06520, United States; Energy Sciences Institute, Yale University, West Haven, Connecticut 06516, United States;* orcid.org/0000-0003-4409-2034; Email: hailiang.wang@yale.edu

Authors

Bo Shang − *Department of Chemistry, Yale University, New Haven, Connecticut 06520, United States; Energy Sciences Institute, Yale University, West Haven, Connecticut 06516, United States;* orcid.org/0000-0002-2294-6062

Fengyi Zhao − *Department of Chemistry, Emory University, Atlanta, Georgia 30322, United States;* orcid.org/0000-0003-4837-9294

Sa Suo − *Department of Chemistry, Emory University, Atlanta, Georgia 30322, United States;* orcid.org/0000-0003-0016-8463

Yuanzuo Gao − *Department of Chemistry, Yale University, New Haven, Connecticut 06520, United States; Energy Sciences Institute, Yale University, West Haven, Connecticut 06516, United States*

Colton Sheehan − *Department of Chemistry, University of Pennsylvania, Philadelphia, Pennsylvania 19104, United States*

Sungho Jeon − *Department of Materials Science and Engineering, University of Pennsylvania, Philadelphia, Pennsylvania 19104, United States*

Jing Li − *Department of Chemistry, Yale University, New Haven, Connecticut 06520, United States; Energy Sciences Institute, Yale University, West Haven, Connecticut 06516, United States;* orcid.org/0000-0001-7538-246X

Conor L. Rooney − *Department of Chemistry, Yale University, New Haven, Connecticut 06520, United States; Energy Sciences Institute, Yale University, West Haven, Connecticut 06516, United States;* orcid.org/0000-0001-7058-568X

https://doi.org/10.1021/jacs.3c13540
J. Am. Chem. Soc. 2024, 146, 2267−2274

Oliver Leitner − *Department of Chemistry, Yale University, New Haven, Connecticut 06520, United States; Energy Sciences Institute, Yale University, West Haven, Connecticut 06516, United States*

Langqiu Xiao − *Department of Chemistry, University of Pennsylvania, Philadelphia, Pennsylvania 19104, United States;* orcid.org/0000-0003-0695-3075

Hanqing Fan − *Department of Chemical and Environmental Engineering, Yale University, New Haven, Connecticut 06520-8286, United States*

Menachem Elimelech − *Department of Chemical and Environmental Engineering, Yale University, New Haven, Connecticut 06520-8286, United States;* orcid.org/0000-0003-4186-1563

Leizhi Wang − *Energy Sciences Institute, Yale University, West Haven, Connecticut 06516, United States;* orcid.org/0000-0003-3876-2441

Gerald J. Meyer − *Department of Chemistry, University of North Carolina at Chapel Hill, Chapel Hill, North Carolina 27599, United States;* orcid.org/0000-0002-4227-6393

Eric A. Stach − *Department of Materials Science and Engineering, University of Pennsylvania, Philadelphia, Pennsylvania 19104, United States;* orcid.org/0000-0002-3366-2153

Thomas E. Mallouk − *Department of Chemistry, University of Pennsylvania, Philadelphia, Pennsylvania 19104, United States;* orcid.org/0000-0003-4599-4208

Complete contact information is available at: https://pubs.acs.org/10.1021/jacs.3c13540

Author Contributions

○B.S. and F.Z. have equal contributions.

Notes

The authors declare no competing financial interest.

■ ACKNOWLEDGMENTS

This work was solely supported as part of the Center for Hybrid Approaches in Solar Energy to Liquid Fuels (CHASE), an Energy Innovation Hub funded by the U.S. Department of Energy, Office of Science, Office of Basic Energy Sciences under Award Number DE-SC0021173. C.S. acknowledges an individual fellowship from the US National Science Foundation Graduate Research Fellowship Program (NSF GRFP, DGE-1845298). The electron microscopy was carried out at the Singh Center for Nanotechnology, which is supported by the NSF National Nanotechnology Coordinated Infrastructure Program under grant NNCI-2025608. Additional support to the Nanoscale Characterization Facility at the Singh Center has been provided by the Laboratory for Research on the Structure of Matter (MRSEC) supported by the National Science Foundation (DMR-1720530).

■ REFERENCES

(1) Jordaan, S. M.; Wang, C. Electrocatalytic conversion of carbon dioxide for the Paris goals. *Nature Catalysis* **2021**, *4* (11), 915−920.

(2) Wang, T.; Wang, Y.; Li, Y.; Li, C. The origins of catalytic selectivity for the electrochemical conversion of carbon dioxide to methanol. *Nano Res.* **2023**, 1 DOI: 10.1007/s12274-023-5653-7.

(3) Kondratenko, E. V.; Mul, G.; Baltrusaitis, J.; Larrazábal, G. O.; Pérez-Ramírez, J. Status and perspectives of CO_2 conversion into fuels and chemicals by catalytic, photocatalytic and electrocatalytic processes. *Energy Environ. Sci.* **2013**, *6* (11), 3112−3135.

(4) Bhattacharjee, S.; Rahaman, M.; Andrei, V.; Miller, M.; Rodríguez-Jiménez, S.; Lam, E.; Pornrungroj, C.; Reisner, E. Photoelectrochemical CO_2-to-fuel conversion with simultaneous plastic reforming. *Nature Synthesis* **2023**, *2* (2), 182−192.

(5) Shan, B.; Vanka, S.; Li, T.-T.; Troian-Gautier, L.; Brennaman, M. K.; Mi, Z.; Meyer, T. J. Binary molecular-semiconductor p−n junctions for photoelectrocatalytic CO_2 reduction. *Nature Energy* **2019**, *4* (4), 290−299.

(6) Rahaman, M.; Andrei, V.; Wright, D.; Lam, E.; Pornrungroj, C.; Bhattacharjee, S.; Pichler, C. M.; Greer, H. F.; Baumberg, J. J.; Reisner, E. Solar-driven liquid multi-carbon fuel production using a standalone perovskite−$BiVO_4$ artificial leaf. *Nature Energy* **2023**, *8* (6), 629−638.

(7) Leung, J. J.; Warnan, J.; Ly, K. H.; Heidary, N.; Nam, D. H.; Kuehnel, M. F.; Reisner, E. Solar-driven reduction of aqueous CO_2 with a cobalt bis(terpyridine)-based photocathode. *Nature Catalysis* **2019**, *2* (4), 354−365.

(8) Roh, I.; Yu, S.; Lin, C. K.; Louisia, S.; Cestellos Blanco, S.; Yang, P. Photoelectrochemical CO_2 Reduction toward Multicarbon Products with Silicon Nanowire Photocathodes Interfaced with Copper Nanoparticles. *J. Am. Chem. Soc.* **2022**, *144* (18), 8002−8006.

(9) Wu, Y.; Jiang, Z.; Lu, X.; Liang, Y.; Wang, H. Domino electroreduction of CO_2 to methanol on a molecular catalyst. *Nature* **2019**, *575* (7784), 639−642.

(10) Zhang, X.; Wu, Z.; Zhang, X.; Li, L.; Li, Y.; Xu, H.; Li, X.; Yu, X.; Zhang, Z.; Liang, Y.; Wang, H. Highly selective and active CO_2 reduction electrocatalysts based on cobalt phthalocyanine/carbon nanotube hybrid structures. *Nat. Commun.* **2017**, *8* (1), 14675.

(11) Shang, B.; Zhao, F.; Choi, C.; Jia, X.; Pauly, M.; Wu, Y.; Tao, Z.; Zhong, Y.; Harmon, N.; Maggard, P. A.; Lian, T.; Hazari, N.; Wang, H. Monolayer Molecular Functionalization Enabled by Acid−Base Interaction for High-Performance Photochemical CO_2 Reduction. *ACS Energy Letters* **2022**, *7* (7), 2265−2272.

(12) Nandal, N.; Jain, S. L. A review on progress and perspective of molecular catalysis in photoelectrochemical reduction of CO_2. *Coordin Chem. Rev.* **2022**, *451*, No. 214271.

(13) Chang, X.; Wang, T.; Yang, P.; Zhang, G.; Gong, J. The Development of Cocatalysts for Photoelectrochemical CO_2 Reduction. *Adv. Mater.* **2019**, *31* (31), No. 1804710.

(14) Wen, Z.; Xu, S.; Zhu, Y.; Liu, G.; Gao, H.; Sun, L.; Li, F. Aqueous CO_2 Reduction on Si Photocathodes Functionalized by Cobalt Molecular Catalysts/Carbon Nanotubes. *Angew. Chem., Int. Ed.* **2022**, *61*, No. e202201086.

(15) Shang, B.; Rooney, C. L.; Gallagher, D. J.; Wang, B. T.; Krayev, A.; Shema, H.; Leitner, O.; Harmon, N. J.; Xiao, L.; Sheehan, C.; Bottum, S. R.; Gross, E.; Cahoon, J. F.; Mallouk, T. E.; Wang, H. Aqueous Photoelectrochemical CO_2 Reduction to CO and Methanol over a Silicon Photocathode Functionalized with a Cobalt Phthalocyanine Molecular Catalyst. *Angew. Chem., Int. Ed.* **2023**, *62* (4), No. e202215213.

(16) Wang, Q.; Pan, Z. Advances and challenges in developing cocatalysts for photocatalytic conversion of carbon dioxide to fuels. *Nano Res.* **2022**, *15* (12), 10090−10109.

(17) Yao, T.; An, X.; Han, H.; Chen, J. Q.; Li, C. Photoelectrocatalytic Materials for Solar Water Splitting. *Adv. Energy Mater.* **2018**, *8* (21), No. 1800210.

(18) Suo, S.; Sheehan, C.; Zhao, F.; Xiao, L.; Xu, Z.; Meng, J.; Mallouk, T. E.; Lian, T. Direct Vibrational Stark Shift Probe of Quasi-Fermi Level Alignment in Metal Nanoparticle Catalyst-Based Metal−Insulator−Semiconductor Junction Photoelectrodes. *J. Am. Chem. Soc.* **2023**, *145* (26), 14260−14266.

(19) Choi, C.; Zhao, F.; Hart, J. L.; Gao, Y.; Menges, F.; Rooney, C. L.; Harmon, N. J.; Shang, B.; Xu, Z.; Suo, S.; Sam, Q.; Cha, J. J.; Lian, T.; Wang, H. Synergizing Electron and Heat Flows in Photocatalyst for Direct Conversion of Captured CO2. *Angew. Chem., Int. Ed.* **2023**, *62*, No. e202302152.

(20) Jiang, S.; Chen, Z.; Chen, X.; Nguyen, D.; Mattei, M.; Goubert, G.; Van Duyne, R. P. Investigation of Cobalt Phthalocyanine at the

Solid/Liquid Interface by Electrochemical Tip-Enhanced Raman Spectroscopy. *J. Phys. Chem. C* **2019**, *123* (15), 9852−9859.
(21) Liu, Z.; Chen, Z.-X.; Jin, B.; Zhang, X. Theoretical studies on the structures and vibrational spectra of Ni, Pd, and Pt phthalocyanines. *Vib. Spectrosc.* **2011**, *56* (2), 210−218.
(22) Dresselhaus, M. S.; Dresselhaus, G.; Saito, R.; Jorio, A. Raman spectroscopy of carbon nanotubes. *Phys. Rep.* **2005**, *409* (2), 47−99.
(23) Filho, A. G. S.; Jorio, A.; Samsonidze, G. G.; Dresselhaus, G.; Saito, R.; Dresselhaus, M. S. Raman spectroscopy for probing chemically/physically induced phenomena in carbon nanotubes. *Nanotechnology* **2003**, *14* (10), 1130.
(24) Clark, M. L.; Ge, A.; Videla, P. E.; Rudshteyn, B.; Miller, C. J.; Song, J.; Batista, V. S.; Lian, T.; Kubiak, C. P. CO_2 Reduction Catalysts on Gold Electrode Surfaces Influenced by Large Electric Fields. *J. Am. Chem. Soc.* **2018**, *140* (50), 17643−17655.
(25) Heo, J.; Ahn, H.; Won, J.; Son, J. G.; Shon, H. K.; Lee, T. G.; Han, S. W.; Baik, M.-H. Electro-inductive effect: Electrodes as functional groups with tunable electronic properties. *Science* **2020**, *370* (6513), 214−219.
(26) Shi, H.; Zhao, B.; Ma, J.; Bronson, M. J., Jr; Cai, Z.; Chen, J.; Wang, Y.; Cronin, M.; Jensen, L.; Cronin, S. B. Measuring Local Electric Fields and Local Charge Densities at Electrode Surfaces Using Graphene-Enhanced Raman Spectroscopy (GERS)-Based Stark-Shifts. *ACS Applied Materials & Interfaces* **2019**, *11* (39), 36252−36258.
(27) Basova, T. V.; Kiselev, V. G.; Schuster, B.-E.; Peisert, H.; Chassé, T. Experimental and theoretical investigation of vibrational spectra of copper phthalocyanine: polarized single-crystal Raman spectra, isotope effect and DFT calculations. *J. Raman Spectrosc.* **2009**, *40* (12), 2080−2087.
(28) Ott, A.; Verzhbitskiy, I. A.; Clough, J.; Eckmann, A.; Georgiou, T.; Casiraghi, C. Tunable D peak in gated graphene. *Nano Research* **2014**, *7* (3), 338−344.
(29) Liu, J.; Li, Q.; Zou, Y.; Qian, Q.; Jin, Y.; Li, G.; Jiang, K.; Fan, S. The Dependence of Graphene Raman D-band on Carrier Density. *Nano Lett.* **2013**, *13* (12), 6170−6175.
(30) Fu, W.; Nef, C.; Knopfmacher, O.; Tarasov, A.; Weiss, M.; Calame, M.; Schönenberger, C. Graphene Transistors Are Insensitive to pH Changes in Solution. *Nano Lett.* **2011**, *11* (9), 3597−3600.
(31) Ang, P. K.; Chen, W.; Wee, A. T. S.; Loh, K. P. Solution-Gated Epitaxial Graphene as pH Sensor. *J. Am. Chem. Soc.* **2008**, *130* (44), 14392−14393.
(32) Lin, F.; Boettcher, S. W. Adaptive semiconductor/electrocatalyst junctions in water-splitting photoanodes. *Nat. Mater.* **2014**, *13* (1), 81−86.
(33) Nellist, M. R.; Laskowski, F. A. L.; Lin, F.; Mills, T. J.; Boettcher, S. W. Semiconductor−Electrocatalyst Interfaces: Theory, Experiment, and Applications in Photoelectrochemical Water Splitting. *Acc. Chem. Res.* **2016**, *49* (4), 733−740.
(34) Lin, F.; Bachman, B. F.; Boettcher, S. W. Impact of Electrocatalyst Activity and Ion Permeability on Water-Splitting Photoanodes. *J. Phys. Chem. Lett.* **2015**, *6* (13), 2427−2433.
(35) Mills, T. J.; Lin, F.; Boettcher, S. W. Theory and Simulations of Electrocatalyst-Coated Semiconductor Electrodes for Solar Water Splitting. *Phys. Rev. Lett.* **2014**, *112* (14), No. 148304.
(36) Thibault, F.; Martinez, R. Z.; Domenech, J. L.; Bermejo, D.; Bouanich, J.-P. Raman and infrared linewidths of CO in Ar. *J. Chem. Phys.* **2002**, *117* (6), 2523−2531.
(37) Hickstein, D. D.; Goldfarbmuren, R.; Darrah, J.; Erickson, L.; Johnson, L. A. Rapid, accurate, and precise concentration measurements of a methanol-water mixture using Raman spectroscopy. *OSA Continuum* **2018**, *1* (3), 1097−1110.
(38) Wu, Y.; Liang, Y.; Wang, H. Heterogeneous Molecular Catalysts of Metal Phthalocyanines for Electrochemical CO_2 Reduction Reactions. *Acc. Chem. Res.* **2021**, *54* (16), 3149−3159.
(39) Li, J.; Shang, B.; Gao, Y.; Cheon, S.; Rooney, C. L.; Wang, H. Mechanism-guided realization of selective carbon monoxide electroreduction to methanol. *Nature Synthesis* **2023**, *2*, 1194−1201.
(40) Rooney, C.; Lyons, M.; Wu, Y.; Hu, G.; Wang, M.; Choi, C.; Gao, Y.; Chang, C.-W.; Brudvig, G.; Feng, Z.; Wang, H. Active Sites of Cobalt Phthalocyanine in Electrocatalytic CO_2 Reduction to Methanol. *Angew. Chem., Int. Ed.* **2023**, No. e202310623.
(41) Kempler, P. A.; Richter, M. H.; Cheng, W.-H.; Brunschwig, B. S.; Lewis, N. S. Si Microwire-Array Photocathodes Decorated with Cu Allow CO_2 Reduction with Minimal Parasitic Absorption of Sunlight. *ACS Energy Letters* **2020**, *5* (8), 2528−2534.
(42) Wakerley, D.; Lamaison, S.; Ozanam, F.; Menguy, N.; Mercier, D.; Marcus, P.; Fontecave, M.; Mougel, V. Bio-inspired hydrophobicity promotes CO_2 reduction on a Cu surface. *Nat. Mater.* **2019**, *18* (11), 1222−1227.
(43) Deshmukh, A.; Boo, C.; Karanikola, V.; Lin, S.; Straub, A. P.; Tong, T.; Warsinger, D. M.; Elimelech, M. Membrane distillation at the water-energy nexus: limits, opportunities, and challenges. *Energy Environ. Sci.* **2018**, *11* (5), 1177−1196.

https://doi.org/10.1021/jacs.3c13540
J. Am. Chem. Soc. 2024, 146, 2267−2274